



■ BONE BIOLOGY

Increased sclerostin associated with stress fracture of the third metacarpal bone in the Thoroughbred racehorse

**N. Hopper,
E. Singer,
F. Henson**

University of
Cambridge, United
Kingdom

Objectives

The exact aetiology and pathogenesis of microdamage-induced long bone fractures remain unknown. These fractures are likely to be the result of inadequate bone remodelling in response to damage. This study aims to identify an association of osteocyte apoptosis, the presence of osteocytic osteolysis, and any alterations in sclerostin expression with a fracture of the third metacarpal (Mc-III) bone of Thoroughbred racehorses.

Methods

A total of 30 Mc-III bones were obtained; ten bones were fractured during racing, ten were from the contralateral limb, and ten were from control horses. Each Mc-III bone was divided into a fracture site, condyle, condylar groove, and sagittal ridge. Microcracks and diffuse microdamage were quantified. Apoptotic osteocytes were measured using TUNEL staining. Cathepsin K, matrix metalloproteinase-13 (MMP-13), HtrA1, and sclerostin expression were analyzed.

Results

In the fracture group, microdamage was elevated 38.9% (SD 2.6) compared with controls. There was no difference in the osteocyte number and the percentage of apoptotic cells between contralateral limb and unraced control; however, there were significantly fewer apoptotic cells in fractured samples ($p < 0.02$). Immunohistochemistry showed that in deep zones of the fractured samples, sclerostin expression was significantly higher ($p < 0.03$) than the total number of osteocytes. No increase in cathepsin K, MMP-13, or HtrA1 was present.

Conclusion

There is increased microdamage in Mc-III bones that have fractured during racing. In this study, this is not associated with osteocyte apoptosis or osteocytic osteolysis. The finding of increased sclerostin in the region of the fracture suggests that this protein may be playing a key role in the regulation of bone microdamage during stress adaptation.

Cite this article: *Bone Joint Res* 2018;7:94–102.

Keywords: Sclerostin, Microdamage, Bone fracture, Apoptosis, Osteocyte

■ N. Hopper, Research Associate, Department of Surgery, University of Cambridge,

■ F. Henson, Senior Lecturer in Equine Surgery, Department of Veterinary Medicine, University of Cambridge, Madingley Road, Cambridge CB3 0ES, UK and Division of Trauma and Orthopaedic Surgery, University of Cambridge, Hills Road, Cambridge BC2 0QQ, UK.

■ E. Singer, Senior Lecturer in Equine Orthopaedics, Department of Musculoskeletal Biology, Institute of Ageing and Chronic Disease, School of Veterinary Medicine, Leahurst, Chester High Road, Neston CH64 6SW, UK.

Correspondence should be sent to N. Hopper; email: niina.hopper@gmail.com

doi: 10.1302/2046-3758.71.BJR-2016-0202.R4

Bone Joint Res 2018;7:94–102.

Article focus

- This study aims to identify evidence for nonapoptotic bone remodelling mechanisms by osteocytes in microdamaged bone.
- Secondly, this study investigates whether the Wnt signalling protein sclerostin is altered in fractured bone.

Key messages

- This study found that targeted remodelling in the bone is not dependent on osteocyte apoptosis.

- The key finding is a marked increase in the Wnt signalling inhibitor sclerostin, suggesting that this protein may be produced at sites of high bone density in order to reduce further bone deposition, therefore playing a role in the regulation of bone microdamage during stress adaptation.

Strengths and limitations

- This study has a strong clinical sample size ($n=30$) of distal Mc-III bones, both fractured and nonfractured, from Thoroughbred horses.

- This study indicates that microdamage in the racehorse has a fundamentally different pathological process to that modelled in small rodent animals, and these results should be further validated in a human fracture model.

Introduction

Long bone fractures in horses have significant welfare and economic implications for the horseracing industry. A clear understanding of their aetiology and pathogenesis is key for the prevention of fractures. In horses, long bone fractures occur because of either a one-off overload incident or repetitive microdamage and subsequent weakening, usually associated with high-intensity exercise. Fractures resulting from microdamage are commonly termed 'stress fractures' and often present as catastrophic fractures when the horse is exercising.¹ In the United Kingdom, it has been shown that lameness was the most important cause of days lost from training in two- or three-year-old Thoroughbred horses, and that stress fractures are the most significant cause of this lameness, with an incidence of 1.48/100 and 1.43/100 per horse month in two- and three-year-old horses, respectively.^{2,3} A number of bones are affected by stress fractures, including the carpal bones, proximal sesamoid bones, tibia, and humerus, with the distal condyle of the third metacarpal bone (Mc-III) being one of the most common sites to be affected.^{4,5}

A Thoroughbred racehorse runs at speeds exceeding 15 m/s, applying highly repetitive surface strains of > 5000 $\mu\epsilon$ to the Mc-III,⁶ which in turn leads to microdamage accumulating in the joint surface and adjacent subchondral bone plate.^{7,8} The histological damage can be seen in two distinct forms: linear microcracks and diffuse microdamage.⁹⁻¹¹ During these high-intensity exercise regimes, repair of the microdamage is undertaken by bone remodelling, which requires the coupling of bone resorption and formation, in order to maintain mineral homeostasis, adapt to mechanical change, and repair damage. The latter two scenarios are site-specific and are termed 'targeted bone remodelling'.¹²

A stress fracture is likely to be the result of inadequate targeted bone remodelling responding to microdamage. It occurs when bone resorption exceeds bone formation, resulting in weakened bones and the propagation of fracture lines. Targeted bone remodelling is controlled by osteocytes, the key roles of which in bone homeostasis include regulation of bone formation, control of bone resorption (via both apoptotic and nonapoptotic pathways), receptor activator of nuclear factor kappa-B ligand (RANKL)-mediated signals, and the transduction of mechanical signals to induce an appropriate biological response.^{13,14} The regulation of bone formation by osteocytes is predominately via sclerostin production, a Wnt signalling inhibitor that inhibits bone formation,¹⁵ which is in turn modulated by local load.¹⁶ Inhibition of

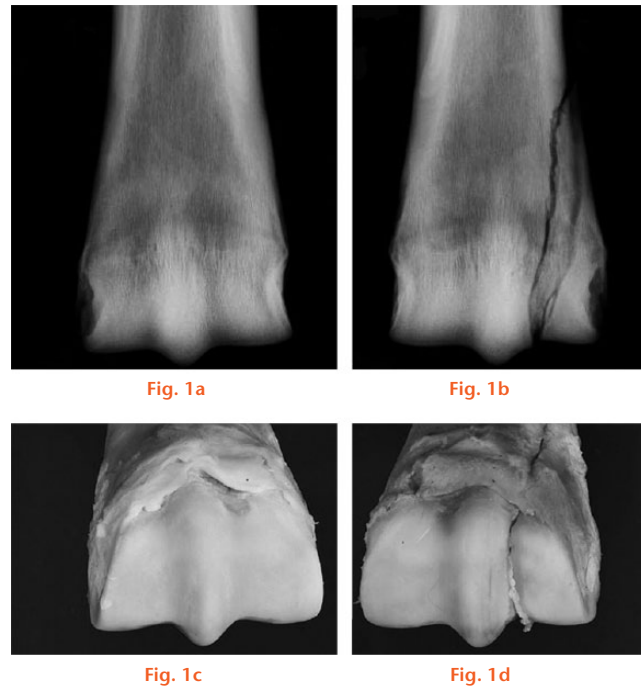
sclerostin with neutralizing antibodies has been shown to accelerate fracture healing¹⁷ and sclerostin knockout mice have been demonstrated to have faster healing fractures,¹⁸ suggesting sclerostin may inhibit bone healing *in vivo*. Nonapoptotic mechanisms of bone remodelling include direct remodelling of the perilacunar bone ('osteocytic osteolysis').¹³ Osteocytic osteolysis takes place via the production by osteocytes of degradative enzymes such as cathepsin K,¹⁹ metalloproteinase-13 (MMP-13),²⁰ and the serine protease HtrA1,²¹ as well as the classic osteoclast enzyme, tartrate-resistant acid phosphatase (TRAP). These enzymes can be used as surrogate markers for this process. However, while some studies on the Thoroughbred racehorse have investigated the role of osteocyte apoptosis in stress fractures, no studies have been performed in horses to investigate Wnt signalling pathways or direct remodelling in microdamaged bone.

This report identifies evidence for nonapoptotic bone remodelling mechanisms by osteocytes in microdamaged bone, and investigates whether the Wnt signalling protein sclerostin is altered in microdamaged bone.

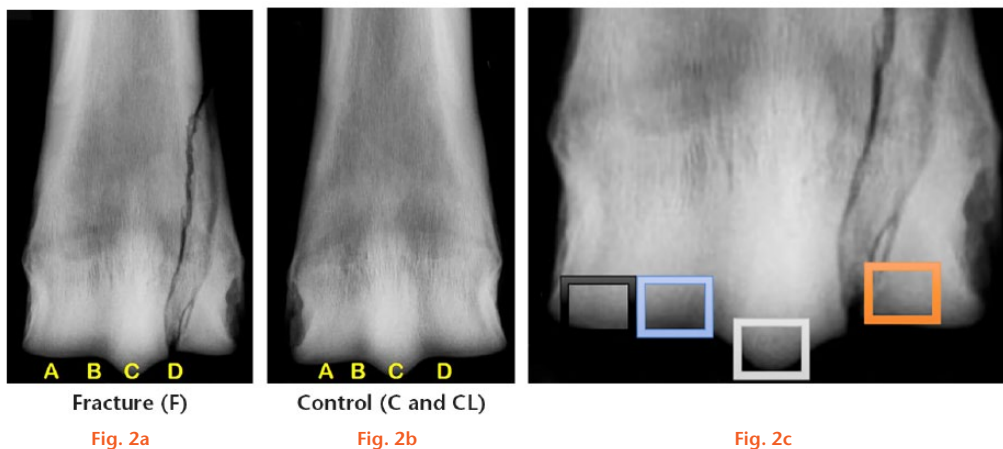
Materials and Methods

Animals. Mc-III bones were obtained from Thoroughbred racehorses that had been euthanized on racetracks in California (in one of Stockton, Arcadia, Berkeley, Inglewood, or Pomona), United States following a catastrophic fracture, and were collected as part of the California Horse Racing Board post-mortem programme (Fig. 1). The study groups were: Group F, distal Mc-III lateral condylar fractures that occurred on the racetrack immediately prior to euthanasia (n=10), six of which were left-leg fractures and four of which were right-leg fractures; and the contralateral (CL) Group, distal Mc-III contralateral (uninjured) legs from horses in Group F (n=10). All horses raced on anticlockwise racecourses, so the increased stress was on the left leg. Horses with bilateral fractures were excluded, as were those with concurrent fracture pathology, such as pre-existing stress fractures. A control group, Group C, consisting of distal Mc-III, comprised Thoroughbred horses who had sustained fatal, non-orthopaedic injuries on the racetrack (n=10). For Groups F and CL, the mean age was 4.1 years (SD 1.2); for Group C, the mean age was 3.9 years (SD 1.5). For all samples, distal thoracic limbs were transected at the level of the carpal bone and stored at -20°C after euthanasia. The time to euthanasia was ten minutes, and samples were preserved frozen for up to six hours post-mortem.

Specimen preparation. A frontal plane bone block of the distal Mc-III,^{22,23} approximately 1 cm thick, was prepared using a band saw. The bone block of the joint surface was then divided into four pieces using sagittal plane cuts to create separate blocks of each of the regions of interest: lateral condylar fracture site, medial condyle, medial condylar groove, and sagittal ridge (Fig. 2).²³



Dorsopalmar (anterior/posterior) radiographs of a) intact third metacarpal bone (Mc-III) and b) fractured bone of same horse. Photograph of articular surfaces of c) intact bone and d) fractured Mc-III. Left medial and right lateral side.



Dorsopalmar radiographs of a) fractured third metacarpal bone and b) control and contralateral bone. The different regions used in the analysis of staining are shown. A, medial condyle; B, medial condylar groove; C, sagittal ridge; D, lateral condylar fracture site. In c), the sampling site regions are shown, corresponding to A to D in a) and b).

Preparation of tissue sections. For each site, both frozen and polymethyl methacrylate (PMMA) sections were obtained. Frozen samples were subsequently used for immunohistochemistry, and PMMA samples were used for histological staining. Frozen sections were produced by embedding optimal cutting temperature (OCT) Cryo embedding compound (SDLAMB/OCT, Fisher Healthcare, Norwich, United Kingdom) and snap-freezing in liquid nitrogen. Sections of 10 μ m thickness were produced through the central portion of the bone block using a cryostat. The unfixed and non-demineralized tissue cryosections were tape-transferred and glued to slides with ultraviolet-sensitive glass adhesive.

To visualize the microdamage within the bones, the whole bone was stained prior to sectioning, in order to ensure that damage produced during the processing would not be stained and would therefore be excluded from damage quantification.^{23,24} This was performed by the PMMA sections of the bone block being fixed in 70% ethanol and bulk-stained in 1% basic fuchsin (JT Baker Basic Fuchsin, JTB-B660-03; Surechem Products Ltd, Ipswich, United Kingdom) in a graded series of ethanols (80%, 90%, 100%) for a total staining time of 18 days, allowing thorough penetration of staining and dehydration of the bones. After embedding in PMMA, 20 μ m calcified oblique frontal plane sections were prepared from the

centre of each block. This basic acid fuchsin technique stains microcracks and diffuses matrix damage that existed before histological sectioning.²⁵

Visualization of microdamage. The sections of PMMA were dehydrated, mounted in DPX mounting medium (44581; Sigma-Aldrich Co. Ltd, London, United Kingdom), and dried. Sections were imaged using a fluorescence microscope (Leica DMRB, Leica, Wetzlar, Germany), and over 200 microscope images per section were stitched together using Surveyor image analysis software (Objective Imaging Ltd, Cambridge, United Kingdom) and subsequently analyzed with ImageJ software.²⁶ The number of microcracks was quantified by expressing the number of cracks per section, normalized to the total length of the cartilage/subchondral bone interface for each section. Branched cracks were counted as one crack and each section was scored blind by the same observer to ensure consistency between data collection. Diffuse damage was quantified by expressing the number of discrete areas of diffuse damage section normalized to the total length of the cartilage/subchondral bone interface for each section.

Quantification of osteocyte apoptosis. The prevalence and location of apoptotic osteocytes/osteoblasts were detected using the DeadEnd fluorometric terminal deoxynucleotidyl transferase (TdT) dUTP nick end labelling (TUNEL) System (G3250; Promega, Madison, Wisconsin).

The cryosections were fixed by immersing slides in freshly prepared 4% methanol-free formaldehyde solution in Phosphate Buffered Saline (PBS) (pH 7.4) for five minutes at room temperature. The slides were then washed by immersing in PBS for five minutes and then incubated in proteinase K solution (20 µg/ml) to make the tissue sections permeable. The sections were then incubated with nucleotide mix and recombinant terminal deoxynucleotidyl transferase (rTdT) enzyme at 37°C for 60 minutes and the controls sections, without the rTdT enzyme, were incubated at the same temperature for the same period. The sections were then mounted in VECTASHIELD + 4',6-diamidino-2-phenylindole (DAPI) (Vector Lab Cat. H-1200, Vector Laboratories, Maravai LifeSciences, Peterborough, United Kingdom) to stain nuclei and were immediately analyzed under a fluorescence microscope, Nikon Ti-E Perfect Focus System (Nikon UK Limited, Surrey, United Kingdom), using a standard fluorescein filter set to view the green fluorescence of fluorescein at 520 nm (SD 20) and blue DAPI at 460 nm under a 10× objective. All the nuclei of osteocytes (both live DAPI at 460 nm and dead green fluorescein at 520 nm) were counted with ImageJ software using particle analysis in the nucleus counter plugin. All the dead cells were quantified, counting only green fluorescein nuclei with ImageJ software, using particle analysis in the nucleus counter plugin. From each site, a representative area of 0.1 mm² (about 380 × 280 µm) was analyzed from the surface of four different anatomical

regions (condyle, condylar groove, sagittal ridge, and fracture site).

Immunohistochemistry. Frozen sections were labelled with Rb pAb sclerostin (Ab63097; Abcam, Cambridge, United Kingdom), Rb pAb HtrA1 (Ab38611; Abcam), Ms mAb cathepsin K (Ab66267; Abcam), and Ms mAb MMP-13 (Ab3208; Abcam), using anti-Mouse IgG (071M6210; Sigma) and anti-Rabbit IgG (B8895; Sigma) secondary antibodies. A horseradish peroxidase detection method was used to detect staining and sections were then counterstained with toluidine blue or methyl green to allow visual identification of the cells. Sections were examined using bright field optics on a Leica DMRXA2 (Leica) with a QImaging Retiga EX fast 1394 camera system (QImaging, Surrey, British Columbia, Canada) under a 60× and 100× objective. At each of the anatomical sites, the total number of osteocytes and the positively labelled osteocytes were quantified in an area of 1 mm² in the subchondral bone (immediately beneath the cartilage/bone interface ('surface zone')) and in an area of 1 mm² immediately below this ('deep zone') 5 mm to 10 mm below the surface zone.

Statistical analysis. All samples were processed to collect four technical replicates for each experiment and the data are presented as mean and standard deviation (SD) with the significance level set at $p < 0.05$. The data were evaluated using Student's *t*-test, analysis of variance (ANOVA), and nonparametric Mann-Whitney U test to determine statistically significant differences with GraphPad Prism 5 software (GraphPad Software Inc., La Jolla, California).

Results

Microdamage quantification. This study identified both microcracks and diffuse damage in the samples studied (Fig. 3). There was significantly increased microcrack damage/area in the lateral condylar fracture site of Group F (7.04 cracks/mm² (SD 2.91)), compared with Group CL (3.18 cracks/mm² (SD 4.26)) and Group C (2.93 cracks/mm² (SD 3.85)), $p=0.002$ and $p=0.005$, respectively. The *p*-value for Group F was not significant. When the total microcrack damage was compared against the other three sites, there was no significant difference. Nor was there any significant difference between and of the groups at any site in the amount of diffuse damage/area, with Group F having 3.43 (SD 1.5) discrete areas of staining, compared with 2.92 (SD 1.45) in Group CL and 2.55 (SD 1.67) in Group C.

Quantification of apoptosis. The DeadEnd fluorometric apoptosis analysis detected apoptotic cells in all samples studied (Fig. 4). When data from all four sites were pooled, there were significantly fewer apoptotic osteocytes in Group F compared with Group CL ($p=0.002$), but there was no difference detected in the percentage of apoptotic osteocytes when Groups F and CL were compared with Group C. The difference was greatest on the sagittal ridge where the rate of apoptotic cells was 22.2%

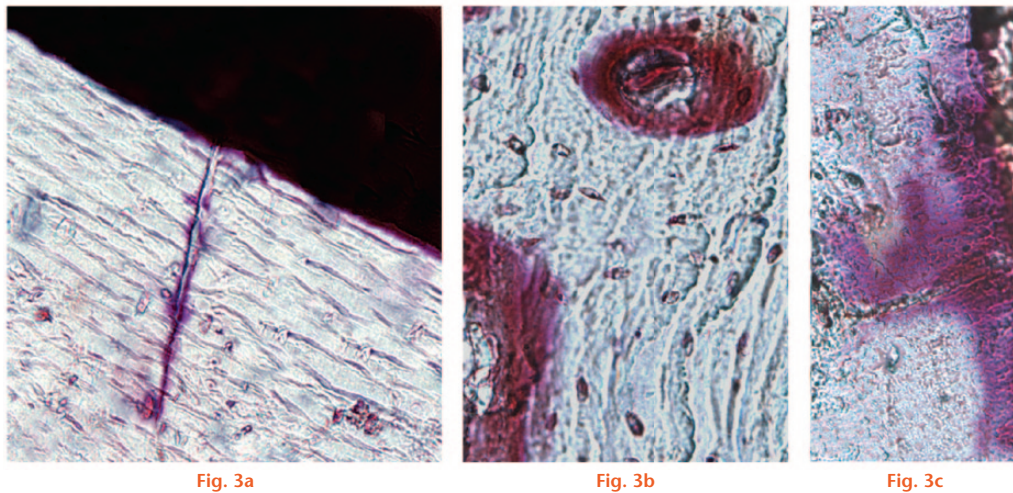


Fig. 3a

Fig. 3b

Fig. 3c

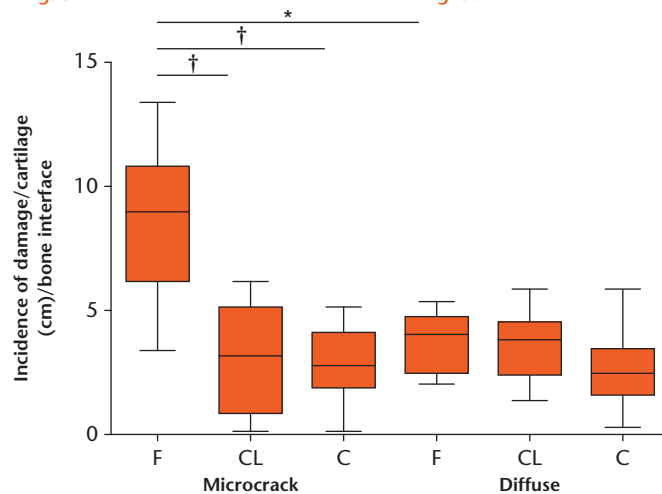


Fig. 3d

Representative micrographs of acid fuchsin-labelled structures in metacarpal bones: a) linear microcrack extending from articular surface; b) staining around blood vessels; and c) diffuse microdamage extending from articular surface. d) Graph showing the amount of damage per surface area of section for microcracks and diffuse damage. There was no difference in the amount of diffuse damage quantified in the three groups; however, there was a statistically significant difference between the amount of microcrack damage/surface area in the lateral condyle (site D, Figure 2) compared with both contralateral and control bones. Scale bar 100 μ m. F, fractured bones; CL, contralateral bones; C, control bones. * $p \leq 0.5$; † $p \leq 0.005$.

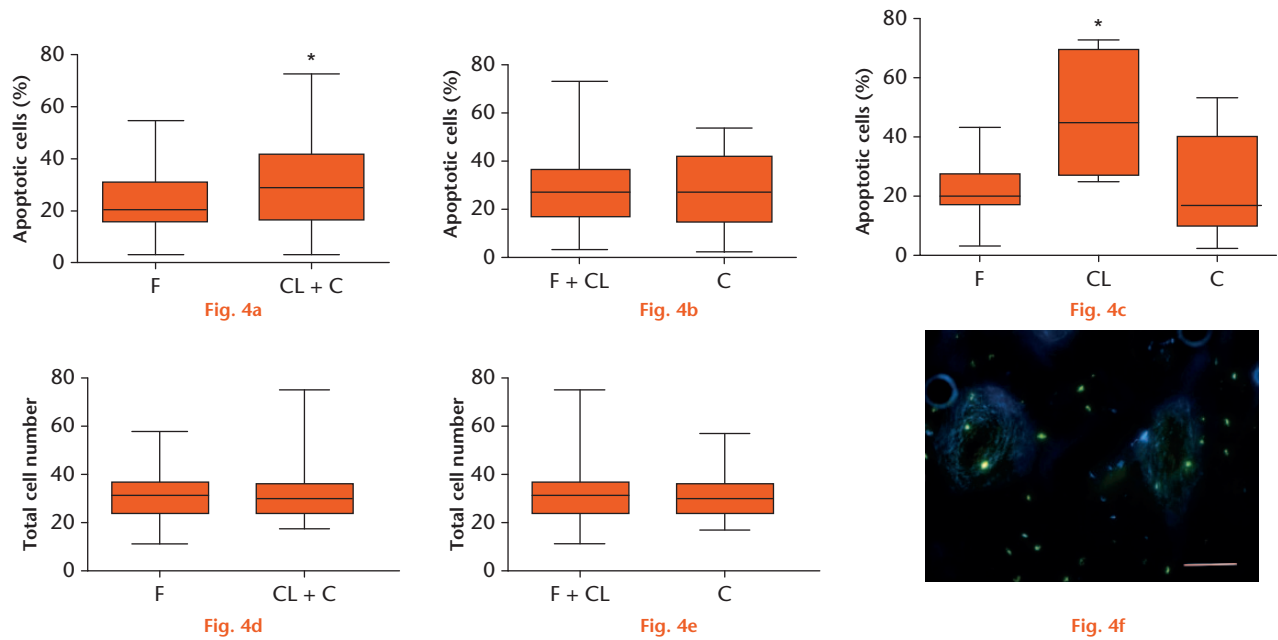
(SD 11.0) in Group F compared with 47.0% (SD 19.6) in Group CL ($p=0.007$).

Enzyme immunohistochemistry. Matrix metalloproteinase-13 (MMP-13), HtrA1, and cathepsin K immunoreactivity were detected in all samples studied. Positive staining was detected in the cytoplasm of the osteocytes in the bone. MMP-13, HtrA1, and cathepsin K immunoreactivity was not different among groups or anatomical sites (Fig. 5).

Sclerostin immunolocalization. Sclerostin immunoreactivity was detected in all samples studied (Fig. 6). Positive staining was detected in the cytoplasm of the osteocytes in the bone. No staining was detected in the cartilage or within the blood vessels. No differences between sites were detected, except in the lateral condylar fracture site groove. At this site, sclerostin immunohistochemistry showed that in the subchondral bone under the articular surface ('surface zone'), staining was in the range of 3.9%

(SD 2.9) of osteocytes staining positive for sclerostin in all samples studied. In the deep zone, however, sclerostin immunohistochemistry showed that there was a significant increase in positive staining in Group F compared with Group CL, with a mean of 24.4% (SD 19.4) of osteocytes staining positive for sclerostin ($p=0.03$) (Fig. 7). In Group F samples, there was a 4.5-fold increase ($p=0.03$) in sclerostin protein-positive cells in the deep zone (24.4%) compared with the cartilage and bone interface (5.4%). In Group CL samples, there was no change in the sclerostin protein between surface and deep zones (2.3% and 3.1%, respectively) (Fig. 7).

In Group C, there was no change in the sclerostin protein between surface and deep zones (9.5% and 10.5%, respectively). However, in the deep zone there was a 2.3-fold increase in sclerostin protein-positive cells in Group F (24.4%) compared with Group C (10.5%). Additionally, in the deep zone CL there was a 7.9-fold increase ($p=0.03$)



Graphs showing: a) quantification of apoptosis within osteocytes in nonfractured and fractured samples; b) raced and non-raced samples; and c) samples from the sagittal ridge. There is a statistically significant difference in the numbers of apoptotic cells ($p < 0.05$) between fractured and nonfractured samples (a) and in the numbers of apoptotic cells on the sagittal ridge, with a significant increase in apoptotic cells in the contralateral limb samples (c). No difference was recorded in the numbers of osteocytes in the samples d) and e). f) Representative microscope image of a fluorometric TUNEL apoptosis analysis. Blue stain shows live cell nuclei, green stain shows apoptotic cells. Scale bar 100 μm. F, fractured bones; CL, contralateral bones, C, control bones.

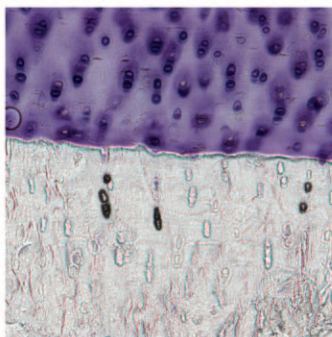


Fig. 5a

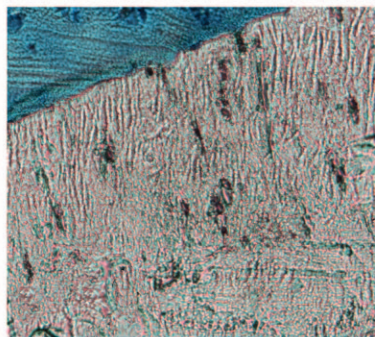


Fig. 5b

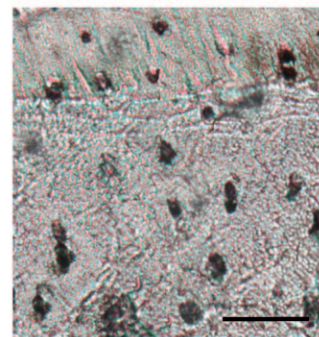


Fig. 5c

Representative photomicrographs of immunohistochemistry in osteocytes in the subchondral bone: a) MMP-13, b) cathepsin K, and c) HTR1A1. Osteocytes stained positively are seen as black cells in the fractured samples. In a), the cartilage is stained with toluidine blue; in b), the cartilage is stained with methyl green. Scale bar 100 μm.

in sclerostin protein-positive cells in Group F (24.4%) compared with Group C (3.1%) (Fig. 7).

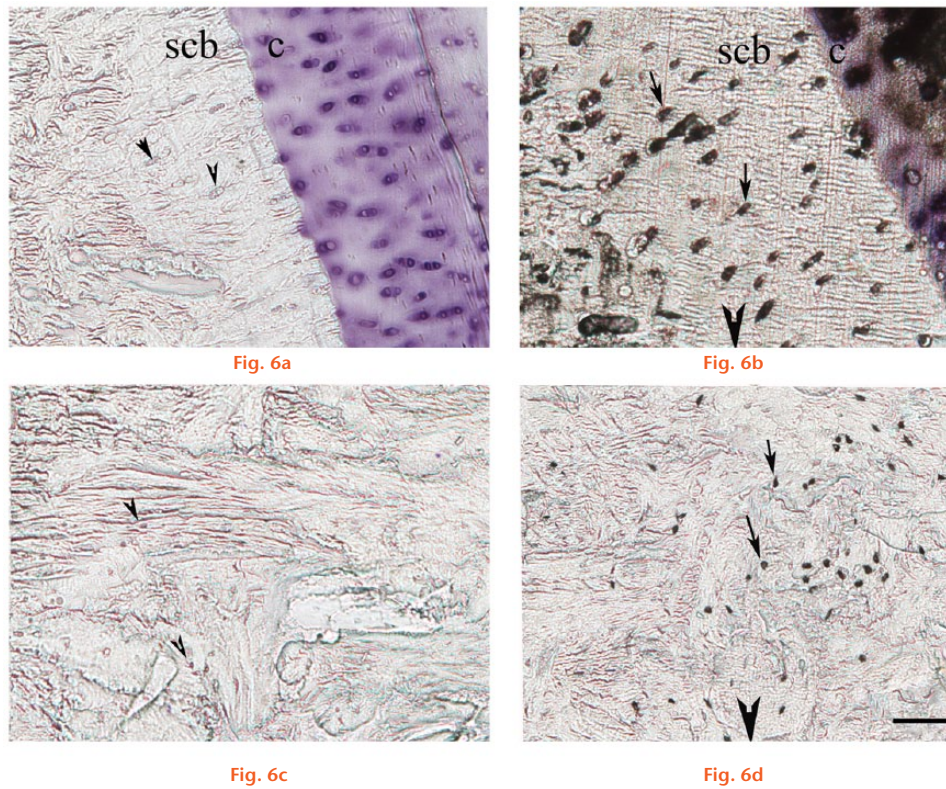
Discussion

In this study, we have shown that osteocyte apoptosis does not increase in regions of microdamage in the Mc-III of Thoroughbred racehorses that sustain fatal lateral condylar fractures. We have demonstrated increased levels of a Wnt signalling inhibitor protein, sclerostin, associated with the fracture line in the fractured bones, but there was no evidence of osteocytic osteolysis in these samples. Our results suggest therefore that Wnt signalling pathways may be important in the aetiology and pathogenesis of

microdamage-induced stress fractures in Thoroughbred racehorses.

Microdamage has been documented in Thoroughbred racehorse fractures as evidence of prefracture pathology.^{27,28} In our study, we have confirmed that the microdamage is similar to that previously reported,^{22,25,27,28} by presectioning staining of all the samples with acid fuchsin and thus ensuring that the microdamage identified was not caused by sample preparation.²⁵ We have identified a mean of 7.04 microcracks/mm² (SD 2.91) joint surface in fractured bones, consistent with the findings of Riggs et al.²²

It has been proposed that the development of linear fracture microcracks through repetitive experimental



Representative photomicrographs of sclerostin immunohistochemistry: a) subchondral bone area control sample; b) subchondral area fracture sample; c) deep zone control sample; and d) deep zone fracture sample. Osteocytes – arrowheads in a) and c) – stained positively for sclerostin are seen as black cells in b) and d) (Group F) and are shown by black arrows. In a), the cartilage is stained with toluidine blue. Scale bar 100 μm . c, cartilage; scb, subchondral bone. The cartilage is stained with toluidine blue and is visible in a) and b). The fracture site is to the bottom of the figures in b) and d) (black arrowhead).

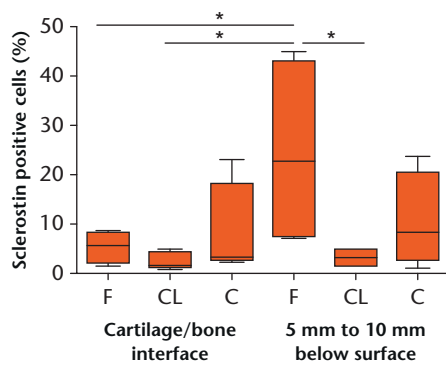


Fig. 7a

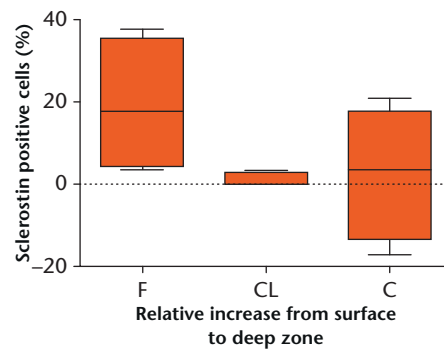


Fig. 7b



Fig. 7c

Quantification of sclerostin immunohistochemistry within osteocytes in fractured (F), contralateral (CL) and control limbs (C). There is a significant increase ($*p < 0.05$) in sclerostin immunoreactivity in the deep zone of the fractured bone. In the photograph, the approximate site of the cartilage/bone interface region (white arrow) and the deeper region is indicated (black arrow).

loading is associated with a loss of osteocyte viability in the region of the microcrack and in the areas that subsequently formed resorption spaces.^{25,29} This has led to the concept that the osteocyte has a role as a mechanoreceptor in bone, sensing load and regulating bone adaptation.¹⁶ A number of small-animal, *in vivo* studies have demonstrated that, in acute models, seven to ten days after fracture, osteocytes regulate bone formation through an apoptosis-mediated mechanism.³⁰⁻³² This mechanism

is currently considered to underlie the control of targeted remodelling of microdamage. However, these acute small-animal experiments, primarily conducted in the rat ulnar fatigue damage model, evaluated very different events compared with the chronic, high-velocity overloading of the Mc-III experienced by the Thoroughbred racehorse and may determine why, in this study, the naturally occurring microdamage is not associated with osteocyte apoptosis. Our observations agree with previous

studies in the equine distal Mc-III, where no association between targeted remodelling and osteocyte apoptosis has been demonstrated.^{8,33} Taken together, though, these studies suggest that targeted bone remodelling in the racehorse is not dependent on osteocyte apoptosis, but that an alternative mechanism of regulation may be involved.^{8,33} Indeed, data for the contralateral limb in our study, in which there was high apoptosis but low microdamage, strongly supports this view.

In the rat ulnar model of microdamage, it has been hypothesized that osteocyte apoptosis stimulates bone remodelling initially via osteoclastic resorption.³⁴ However, osteocytes can regulate bone remodelling via other mechanisms, for example, by osteocytic osteolysis and Wnt signalling pathways.³⁵ In osteocytic osteolysis, osteocytes directly resorb their surrounding environment via a cathepsin K- and/or MMP-13-associated mechanism.^{20,36} We did not, however, find an association between cathepsin K, MMP-13, or HtrA1 immunoreactivity and bone damage, which suggests that osteocytic osteolysis through cathepsin K, MMP-13, or HtrA1 pathways is not linked to microdamage in the racehorse.

In contrast, there was evidence for an association between the Wnt signalling pathway and microdamage. Osteocytes regulate bone formation, primarily via their production of the Wnt signalling protein sclerostin, which inhibits bone formation¹⁵ and responds to local load.¹⁶ We have identified sclerostin protein in osteocytes in all the samples we have studied, especially along the fractured line, where there was a marked and significant increase in sclerostin-positive osteocytes, which was unexpected. In rat ulnar models of a stress fracture, sclerostin has been reported to be reduced adjacent to the fracture line,³⁷ although these were acute experiments. The finding that osteocyte apoptosis is not associated with equine microdamage, but is associated with rat ulnar microdamage, suggests that microdamage in the racehorse has a fundamentally different pathological process to that of small animals.

The presence of increased sclerostin associated with a fracture line in equine stress fractures is of real interest. One explanation could be that the increase in sclerostin is a direct result of increased bone density at the site of the microdamage and that sclerostin, an inhibitor of bone formation, is being produced locally to prevent further physiological bone mass increases, which cause increased stiffness and the likelihood of a fracture. Racehorse training does cause increased bone density in the distal Mc-III,^{38,39} and this bone density has been shown to be heterogeneous across the distal Mc-III.³⁹⁻⁴¹ It has been suggested that these bone density gradients within the bone further drive the formation of microdamage.⁴⁰ The observation that sclerostin is increased at the site of the fracture could suggest that sclerostin is being upregulated in order to inhibit excessive bone formation and thus

prevent decreasing bone density gradients, which in turn may ultimately lead to a fracture. However, the fact that the increased sclerostin was only seen in the fractured bones rather than in the contralateral limb, which had experienced similar racing and training conditions, indicates that the increased sclerostin could be an end-stage event associated with a high probability of fracture. Sclerostin is upregulated by unloading of bone ('stress shielding'),^{42,43} and it may be that local unloading caused by heterogeneous bone density changes is acting as the mechanism to drive this increased sclerostin expression. The possibility that sclerostin might play a role in reducing the physiological consequences of 'excessive' bone mass has also been suggested by the finding that constitutive activation of osteocyte β -catenin in mice increased bone mass but also led to significantly increased serum sclerostin levels, which may be a protective mechanism.³⁷

There are several limitations with our study. One is that the samples studied did not accurately determine when the observed increase in sclerostin occurred relative to the fracture. The observed increase in sclerostin could have been produced prior to fracture, between fracture and death, or post-mortem. Sclerostin could be upregulated post-mortem, although the analysis of the other enzymes with the same samples in our study showed no change in the protein levels. On the other hand, mRNA transcription levels are known to alter within minutes after euthanasia.⁴⁴ However, reduced oxygen tension in the body is one of the main changes post-mortem, and hypoxic conditioning has been reported to reduce sclerostin expression, both on a transcript and protein level in osteoblasts, suggesting that sclerostin upregulation post-mortem is therefore unlikely.⁴⁵

The horses included in this study were euthanized within ten minutes of the fracture occurring, which compares favourably with the longer time between naturally occurring fracture and bone sample acquisition in human studies. It has been shown that sclerostin levels in a human fracture haematoma are significantly increased compared with serum levels, indicating that sclerostin is indeed induced by a fracture.⁴⁶ Hence, future studies need to ensure rapid collection and fixation of samples prior to processing. Another limitation of this study is that sclerostin was only investigated in the distal metacarpus. Further work is therefore required to investigate fractures at other anatomical sites and to analyze any relationship between the levels of training and racing and the levels of sclerostin.

In conclusion, this study has shown no evidence of any role being played by osteocyte apoptosis or osteocytic osteolysis in the stress fractures of Mc-III in the Thoroughbred racehorse. However, a marked increase in the Wnt signalling inhibitor sclerostin was detected, suggesting that this protein may be produced to reduce further bone deposition as an end-stage event, in a bone that has been remodelled too far to sustain its integrity.

References

- Parkin TD, Clegg PD, French NP, et al.** Risk of fatal distal limb fractures among Thoroughbreds involved in the five types of racing in the United Kingdom. *Vet Rec* 2004;154:493-497.
- Dyson PK, Jackson BF, Pfeiffer DU, Price JS.** Days lost from training by two- and three-year-old Thoroughbred horses: a survey of seven UK training yards. *Equine Vet J* 2008;40:650-657.
- Owen KR, Dyson SJ, Parkin TD, et al.** Retrospective study of palmar/plantar annular ligament injury in 71 horses: 2001-2006. *Equine Vet J* 2008;40:237-244.
- Radtke CL, Danova NA, Scollay MC, et al.** Fatigue fracture of the condyles of the third metacarpal/third metatarsal bone in Thoroughbred racehorses. *Am J Vet Res* 2003;64:1110-1116.
- Boyde A, Haroon Y, Jones SJ, Riggs CM.** Three dimensional structure of the distal condyles of the third metacarpal bone of the horse. *Equine Vet J* 1999;31:122-129.
- Nunamaker DM, Butterweck DM, Provost MT.** Fatigue fractures in thoroughbred racehorses: relationships with age, peak bone strain, and training. *J Orthop Res* 1990;8:604-611.
- Muir P, McCarthy J, Radtke CL, et al.** Role of endochondral ossification of articular cartilage and functional adaptation of the subchondral plate in the development of fatigue microcracking of joints. *Bone* 2006;38:342-349.
- Muir P, Peterson AL, Sample SJ, et al.** Exercise-induced metacarpophalangeal joint adaptation in the Thoroughbred racehorse. *J Anat* 2008;213:706-717.
- Vakil JJ, O'Reilly MP, Sutter EG, et al.** Knee arthroscopy repair with a continuous barbed suture: a biomechanical study. *J Arthroplasty* 2011;26:710-713.
- Kawcak CE, McIlwraith CW, Norrdin RW, Park RD, Steyn PS.** Clinical effects of exercise on subchondral bone of carpal and metacarpophalangeal joints in horses. *Am J Vet Res* 2000;61:1252-1258.
- Bentley VA, Sample SJ, Livesey MA, et al.** Morphologic changes associated with functional adaptation of the navicular bone of horses. *J Anat* 2007;211:662-672.
- Burr DB.** Targeted and nontargeted remodeling. *Bone* 2002;30:2-4.
- Bonewald LF.** The amazing osteocyte. *J Bone Miner Res* 2011;26:229-238.
- Schaffler MB, Kennedy OD.** Osteocyte signaling in bone. *Curr Osteoporos Rep* 2012;10:118-125.
- Larsson S.** Anti-sclerostin - is there an indication? *Injury* 2016;47(Suppl 1):S31-S35.
- Nguyen J, Tang SY, Nguyen D, Alliston T.** Load regulates bone formation and Sclerostin expression through a TGF β -dependent mechanism. *PLoS One* 2013;8:e53813.
- Ominsky MS, Li C, Li X, et al.** Inhibition of sclerostin by monoclonal antibody enhances bone healing and improves bone density and strength of nonfractured bones. *J Bone Miner Res* 2011;26:1012-1021.
- Li C, Ominsky MS, Tan HL, et al.** Increased callus mass and enhanced strength during fracture healing in mice lacking the sclerostin gene. *Bone* 2011;49:1178-1185.
- Wysolmerski JJ.** Osteocytes remove and replace perilacunar mineral during reproductive cycles. *Bone* 2013;54:230-236.
- Tang SY, Herber RP, Ho SP, Alliston T.** Matrix metalloproteinase-13 is required for osteocytic perilacunar remodelling and maintains bone fracture resistance. *J Bone Miner Res* 2012;27:1936-1950.
- Tsuchiya A, Yano M, Tocharus J, et al.** Expression of mouse HtrA1 serine protease in normal bone and cartilage and its upregulation in joint cartilage damaged by experimental arthritis. *Bone* 2005;37:323-336.
- Riggs CM, Whitehouse GH, Boyde A.** Structural variation of the distal condyles of the third metacarpal and third metatarsal bones in the horse. *Equine Vet J* 1999;31:130-139.
- Muir P, Peterson AL, Sample SJ, et al.** Exercise-induced metacarpophalangeal joint adaptation in the Thoroughbred racehorse. *J Anat* 2008;213:706-717.
- Burr DB, Hooser M.** Alterations to the en bloc basic fuchsin staining protocol for the demonstration of microdamage produced in vivo. *Bone* 1995;17:431-433.
- Bentolila V, Boyce TM, Fyhrie DP, et al.** Intracortical remodelling in adult rat long bones after fatigue loading. *Bone* 1998;23:275-281.
- Schneider CA, Rasband WS, Eliceiri KW.** NIH Image to ImageJ: 25 years of image analysis. *Nat Methods* 2012;9:671-675.
- van Oers RF, van Rietbergen B, Ito K, Huiskes R, Hilbers PA.** Simulations of trabecular remodelling and fatigue: is remodelling helpful or harmful? *Bone* 2011;48:1210-1215.
- Vallance SA, Spriet M, Stover SM.** Catastrophic scapular fractures in Californian racehorses: pathology, morphometry and bone density. *Equine Vet J* 2011;43:676-685.
- Verborgt O, Gibson GJ, Schaffler MB.** Loss of osteocyte integrity in association with microdamage and bone remodelling after fatigue in vivo. *J Bone Miner Res* 2000;15:60-67.
- Cardoso L, Herman BC, Verborgt O, et al.** Osteocyte apoptosis controls activation of intracortical resorption in response to bone fatigue. *J Bone Miner Res* 2009;24:597-605.
- Noble BS, Peet N, Stevens HY, et al.** Mechanical loading: biphasic osteocyte survival and targeting of osteoclasts for bone destruction in rat cortical bone. *Am J Physiol Cell Physiol* 2003;284:C934-C943.
- Vashisith D, Verborgt O, Divine G, Schaffler MB, Fyhrie DP.** Decline in osteocyte lacunar density in human cortical bone is associated with accumulation of microcracks with age. *Bone* 2000;26:375-380.
- Da Costa Gómez TM, Barrett JG, Sample SJ, et al.** Up-regulation of site-specific remodelling without accumulation of microcracking and loss of osteocytes. *Bone* 2005;37:16-24.
- Kennedy OD, Herman BC, Laudier DM, et al.** Activation of resorption in fatigue-loaded bone involves both apoptosis and active pro-osteoclastogenic signaling by distinct osteocyte populations. *Bone* 2012;50:1115-1122.
- Prideaux M, Findlay DM, Atkins GJ.** Osteocytes: the master cells in bone remodelling. *Curr Opin Pharmacol* 2016;28:24-30.
- Qing H, Ardeshirpour L, Pajevic PD, et al.** Demonstration of osteocytic perilacunar/canalicular remodelling in mice during lactation. *J Bone Miner Res* 2012;27:1018-1029.
- Tu X, Delgado-Calle J, Condon KW, et al.** Osteocytes mediate the anabolic actions of canonical Wnt/ β -catenin signaling in bone. *Proc Natl Acad Sci USA* 2015;112:E478-E486.
- Riggs CM, Boyde A.** Effect of exercise on bone density in distal regions of the equine third metacarpal bone in 2-year-old thoroughbreds. *Equine Vet J Suppl* 1999;30:555-560.
- Loughridge AB, Hess AM, Parkin TD, Kawcak CE.** Qualitative assessment of bone density at the distal articulating surface of the third metacarpal in Thoroughbred racehorses with and without condylar fracture. *Equine Vet J* 2017;49:172-177.
- Stover SM, Murray A.** The California Postmortem Program: leading the way. *Vet Clin North Am Equine Pract* 2008;24:21-36.
- Ramzan PH, Powell SE.** Clinical and imaging features of suspected prodromal fracture of the proximal phalanx in three Thoroughbred racehorses. *Equine Vet J* 2010;42:164-169.
- Lin C, Jiang X, Dai Z, et al.** Sclerostin mediates bone response to mechanical unloading through antagonizing Wnt/ β -catenin signaling. *J Bone Miner Res* 2009;24:1651-1661.
- Spatz JM, Wein MN, Gooi JH, et al.** The Wnt inhibitor sclerostin is up-regulated by mechanical unloading in osteocytes in vitro. *J Biol Chem* 2015;290:16744-16758.
- Pozhitkov AE, Neme R, Domazet-Lošo T, et al.** Tracing the dynamics of gene transcripts after organismal death. *Open Biol* 2017;7:160267.
- Genetos DC, Toupadakis CA, Raheja LF, et al.** Hypoxia decreases sclerostin expression and increases Wnt signaling in osteoblasts. *J Cell Biochem* 2010;110:457-467.
- Sarahrudi K, Thomas A, Albrecht C, Aharinejad S.** Strongly enhanced levels of sclerostin during human fracture healing. *J Orthop Res* 2012;30:1549-1555.

Acknowledgement

- We would like to thank Professor Sue Stover for allowing access to the samples.

Funding Statement

- N. Hopper was funded by the Horserace Betting Levy Board. E. Singer and F. Henson have received funds from Higher Education Funding Council of England (HEFCE). This work was supported by the Horserace Betting Levy Board, grant number PRJ-771.

Author Contributions

- N. Hopper: Experimental work, Analyzing the data, Preparing the manuscript.
- E. Singer: Collecting the samples, Designing the project, Preparing the manuscript.
- F. Henson: Designing the project, Analyzing the data, Preparing the manuscript.

Conflicts of Interest Statement

- None declared

© 2018 Hopper et al. This is an open-access article distributed under the terms of the Creative Commons Attribution licence (CC-BY-NC), which permits unrestricted use, distribution, and reproduction in any medium, but not for commercial gain, provided the original author and source are credited.